

# On-Nanoparticle Gating Units Render an Ordinary Catalyst Substrate- and Site-Selective

Minju Kim, Mirosław Dygas, Yaroslav I. Sobolev, Wiktor Beker, Qiang Zhuang, Tomasz Klucznik, Guillermo Ahumada, Juan Carlos Ahumada, and Bartosz A. Grzybowski\*



Cite This: *J. Am. Chem. Soc.* 2021, 143, 1807–1815



Read Online

ACCESS |



Metrics & More

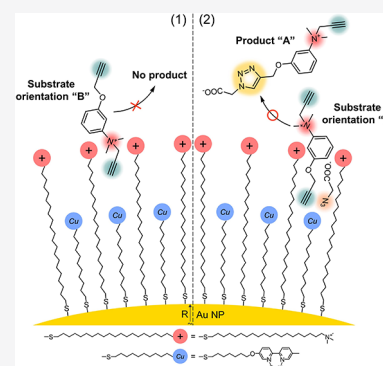


Article Recommendations



Supporting Information

**ABSTRACT:** When an organometallic catalyst is tethered onto a nanoparticle and is embedded in a monolayer of longer ligands terminated in “gating” end-groups, these groups can control the access and orientation of the incoming substrates. In this way, a nonspecific catalyst can become enzyme-like: it can select only certain substrates from substrate mixtures and, quite remarkably, can also preorganize these substrates such that only some of their otherwise equivalent sites react. For a simple, copper-based click reaction catalyst and for gating ligands terminated in charged groups, both substrate- and site-selectivities are on the order of 100, which is all the more notable given the relative simplicity of the on-particle monolayers compared to the intricacy of enzymes’ active sites. The strategy of self-assembling macromolecular, on-nanoparticle environments to enhance selectivities of “ordinary” catalysts presented here is extendable to other types of catalysts and gating based on electrostatics, hydrophobicity, and chirality, or the combinations of these effects. Rational design of such systems should be guided by theoretical models we also describe.



## INTRODUCTION

Enzymes are remarkable for their ability to perform reactions selectively, only on the “fitting” substrates and often only on a specific group even if other, chemically equivalent groups are present in the same substrate.<sup>1</sup> Such substrate- and site-selectivities derive from substrate recognition and preorganization by the loci of the binding pockets that may be quite distant from the catalytic center (Figure 1a). In the last several decades, chemists have strived to build-in similar capabilities into artificial systems.<sup>2–26</sup> Indeed, there have been numerous creative efforts to prepare supramolecular enzyme mimics<sup>2–4</sup> presenting substrate-specific “pockets” based on molecular sieves,<sup>5</sup> cages,<sup>6,7</sup> flasks,<sup>8</sup> cucurbituril derivatives,<sup>9,10</sup> capsules,<sup>11,12</sup> porphyrin-based complexes,<sup>13,14</sup> bidentate ligands with built-in anion recognition sites,<sup>15,16</sup> and several others. These systems can discriminate between substrates based on size,<sup>7,11,14,17</sup> shape,<sup>5,17</sup> transition state conformation,<sup>13</sup> or presence of anionic groups<sup>15,16</sup> and can result in products whose formation is disfavored in typical solution-phase reactions.<sup>8,18,19</sup> For instance, Davis and Jones demonstrated substrate-selective catalysis (or separations) on various types of organic-functionalized molecular sieves (OFMSs) or zeolites.<sup>5,20–25</sup> Groups of Breslow<sup>26–28</sup> (already in the 1990s) and Reek<sup>29–31</sup> and Bayley<sup>32</sup> (more recently) synthesized several elegant systems in which site-selectivity is enhanced by supramolecular interactions mediating preorganization of substrates. Simultaneously, there has been a significant effort on the so-called nanozymes, that is, nanoparticles mimicking the activity of enzymes.<sup>33,34</sup> A significant portion of this

research has focused on biomedical and sensing applications capitalizing on the intrinsic properties of the nanoparticle cores,<sup>35</sup> but there have also been some exciting developments in which the organic ligand shell was engineered to endow substrate specificity,<sup>36,37</sup> to template association of substrates and their subsequent catalytic conversion,<sup>38–40</sup> or to act as a dynamic layer for in-cell<sup>41</sup> or photocontrolled<sup>42</sup> catalysis (for further examples, see recent reviews<sup>33,43</sup>). On the downside, many of these systems achieve only moderate selectivities (especially with respect to equivalent functionalities), are tailored to very specific substrates (Figure 1b), and often require elaborate synthesis.

In this work, we sought to “augment” an otherwise nonselective organometallic catalyst (here, a popular Bipy-Cu(I) for click reaction) and endow it with a high degree of substrate and site-selectivity not by covalent modification but by self-assembly of a macromolecular environment controlling access to the catalytic center. We hypothesized this objective could be achieved by rather simple means, namely, by the formation of a mixed, on-nanoparticle self-assembled monolayer, SAM,<sup>44,45</sup> in which the “gating” end groups of longer ligands would control the approach and orientation of the

Received: September 1, 2020

Published: January 20, 2021



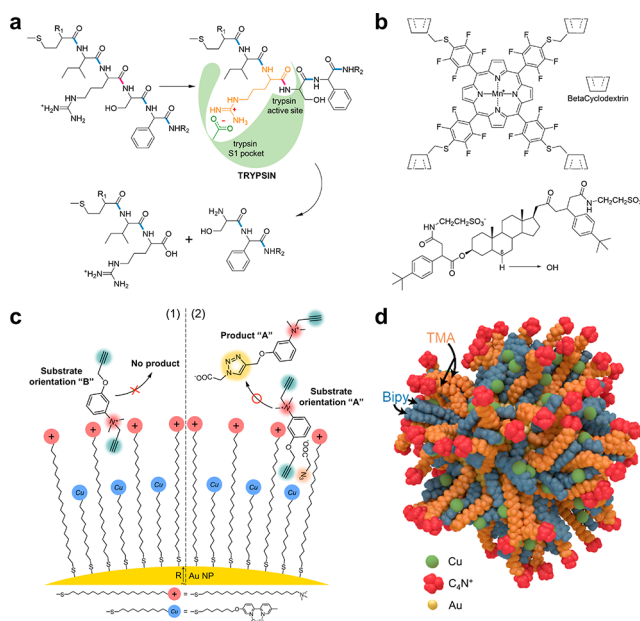


**Figure 1.** Site-selectivity in enzymes and in enzyme mimics. (a) Enzymes can recognize a specific place in a substrate by the use of binding sites sometimes quite distant from the active site. For example, trypsin cleaves only one (colored in red) out of multiple peptide bonds present, and this recognition is mediated by a long, positively charged side chain (in the figure, arginine) that fits into a distant pocket and interacts with a COO<sup>-</sup> group present therein. (b) Example of site-selectivity in an artificial system from Reek's group (figure adapted from ref.<sup>31</sup>). A Mn<sup>III</sup>-porphyrin is functionalized with cyclodextrin (CD) units linked to all meso-phenyl rings. When the termini of an appropriately functionalized steroid derivative bind to the CDs, the steroid's C6  $\alpha$  position is placed precisely at the catalytic center, resulting in hydroxylation of this CH function with regioselectivity exceeding 90%. (c) General principle of on-nanoparticle, charge-based gating. In scenario "1", the positively charged end groups of the longer thiols interact repulsively with the positive group on the incoming substrate (here, a dialkyne partner for the click reaction). Consequently, substrate prefers to enter the ligand shell in orientation illustrated in "2". Only one alkyne group is expected to react with the azide partner at the catalytic center (here, blue circles denoting Cu-Bipy complexes at the end of shorter thiols). (d) A snapshot of a Molecular Dynamics (MD) simulation showing the nanoparticle and its ligand shell, with molecules' contours traced by van der Waals surfaces. Green = copper atoms coordinated to blue Bipy thiols; orange = TMA ligands terminated in red positively charged quaternary nitrogen groups; yellow Au = atoms of the NP core. Not shown are substrate and product molecules. For details of MD simulations, see the Supporting Information (SI), Section S10.3.

substrates with respect to the catalytic centers tethered at the ends of shorter ligands (Figure 1c,d).

Although the on-particle monolayers are significantly less intricate than an enzymes' active sites, they achieve unexpectedly high selectivities. With charged gating groups, these selectivities are as high as  $\sim 100$  for competitive selection from mixtures of negatively and positively charged substrates (Figure 3), and tens to over 100 for the selection between locally equivalent reaction sites (here, triple bonds) within the same substrates (Figure 4). Even for the gating based on weaker, van der Waals interactions, the selectivities are still appreciable, 6–7 fold; in this case, the hydrophobic gating units admit preferentially the more hydrophobic substrates (Figure 6g–i). These experimental findings are substantiated

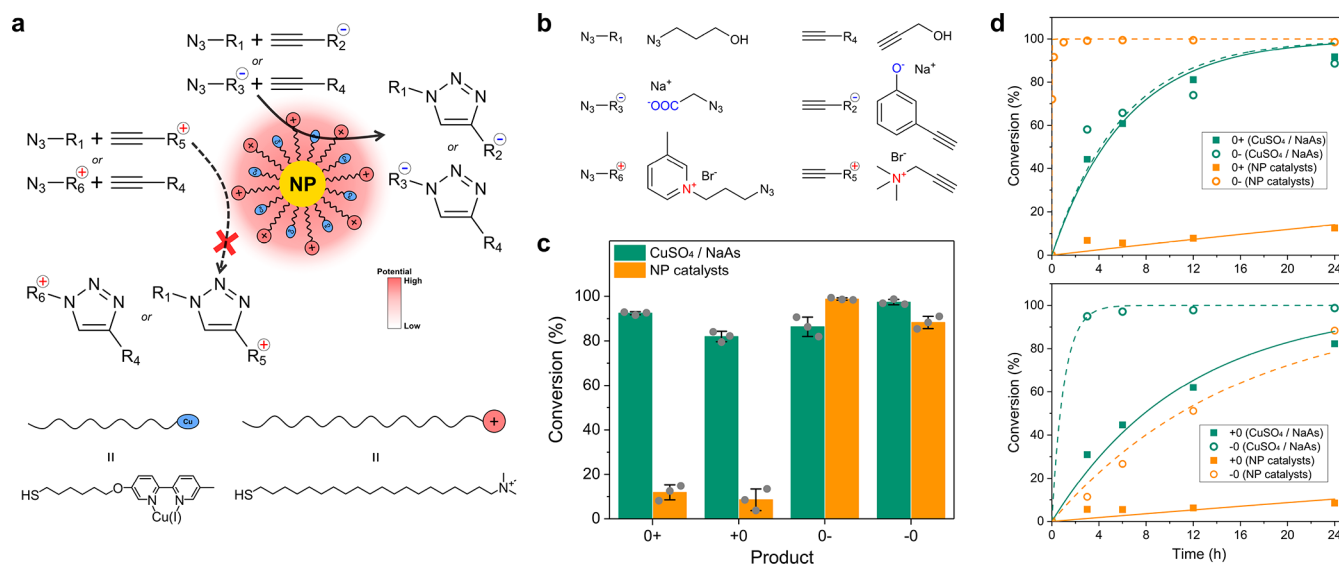
by a theoretical model and simulations accompanying our experiments.

Overall, the system we describe, and others that could be designed based on similar principles for different nonspecific catalysts, can be construed as a hybrid between nanozyme and macromolecular approaches to enzyme mimicry: (i) the nanoparticle supports are important insofar as they present high surface area and can also control the curvature of the monolayer and the overall "enzyme" activity (Figure 6b,c), whereas (ii) the substrate- and site-selectivities derive from the details of the on-particle macromolecular environments.

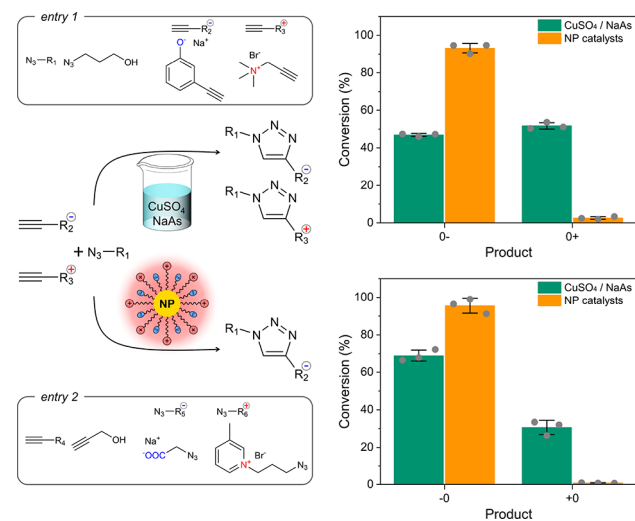
## RESULTS AND DISCUSSION

Figure 1c,d illustrates the architecture of our system whereby gold nanoparticles (typically,  $4.2 \pm 0.4$  nm in size but also  $2.5 \pm 0.3$  nm in some experiments discussed later) support a mixed monolayer comprised of longer alkanethiols terminated in positively charged, "gating" end-groups (*N,N,N*-trimethyl-(20-mercaptoicosanyl) ammonium bromide; TMA) and shorter ligands terminated in bipyridine units (6-((5'-methyl-[2,2'-bipyridine-5-yl]oxy)hexane-1-thiol; Bipy). Once made and purified, the NPs were redispersed in 1:1 v/v water/MeOH mixture at a concentration of  $\sim 5.5 \mu\text{M}$  in terms of the NPs and were then exposed to 10-fold excess CuI, allowing for the coordination of copper to the Bipy units. These Bipy-Cu(I) units were intended to act as catalysts of the so-called "click" reaction, that is, an azide–alkyne cycloaddition leading to 1,4-substituted 1,2,3-triazoles, which is a popular and powerful strategy for covalently joining molecules under a wide range of conditions.<sup>46–48</sup> Afterward, any excess CuI was removed from solution by multiple rounds of centrifugation and methanol was removed by evaporation to yield  $\sim 11 \mu\text{M}$  suspension of NPs in water. Analyses by inductively coupled plasma atomic emission spectroscopy (ICP-AES) showed that (i) concentrations of Cu in solution right after the synthesis and CuI centrifugation, after 24 h, and also after using NPs for click reactions were all below detection limit, and (ii) Cu was localized on the NPs and the measured ratio of Au to Cu matched the one expected for the ca. 50% content of Bipy-Cu(I) units in the on-particle ligand shells. Additional control experiments evidenced only residual catalysis for CuI-purified solutions (nonselective conversions  $\sim 1\%$  at 24 h). Also, AuNPs covered with only TMA, and no Bipy ligands showed no catalytic conversion, excluding the possibility of Cu salts adsorbing onto the NPs via the so-called salt adsorption.<sup>49,50</sup> For details of all these experiments, see the SI, Sections S7 and S8.

We emphasize six important aspects of the system's design. First, The TMA thiols were chosen as gating units because they retain positive charge and the AuNPs they stabilize remain soluble in water irrespective of pH. Second, with TMA thiols shorter than Bipy thiols, the NP suspensions remain stable prior to the addition of CuI but, after such addition, they rapidly flocculate, suggesting some form of "cross-linking" via the Bipy-Cu(I) units (perhaps by the formation of binuclear complexes, see<sup>51–53</sup>). Third, increasing the fraction of Bipy-Cu(I) in the monolayer lowers the particles' solubility in water—the  $\sim 1:1$  ratio we used here appears to be an optimal trade-off between high catalyst loading and NP stability. Fourth, because of electrostatic repulsions between the TMA head-groups, the TMA thiols are unlikely to phase-separate and form distinct patches on NP surfaces—in fact, computer simulations summarized in Figure S92 indicate that such



**Figure 2.** Selectivity for negatively- vs positively- charged substrates. (a) Scheme of the nanoparticle, the incoming substrates, and possible products. Molecular details of the ligands are shown at the bottom. Red glow around the particle indicates electrostatic potential due to positively charged TMA head-groups. (b) Specific substrates used and (c) conversions observed for different pairs of substrates on nanoparticles (orange bars) and for the copper catalysts dispersed in solution (green bars; same Cu concentration as for NPs). “0” means uncharged substrate; “+” or “−” indicate, respectively, positively or negatively charged substrates. The first symbol in the pair denotes azide and the second, alkyne. Error bars are standard deviations from three independent experiments (whose individual outcomes are quantified by gray markers in the histograms). (d) Kinetic plots tracing concentrations of products from panel (c) in the function of time. Lines are exponential fits to experimental data.



**Figure 3.** Experiments with “competing” substrates. Substrates of both polarities (alkynes in “entry 1” and azides in “entry 2”) compete for reaction with a neutral azide/alkyne. Histograms on the right evidence that while  $\text{CuSO}_4/\text{NaAs}$  catalyst (green bars) does not show pronounced preference for negatively charged substrates, the NP catalyst—carrying the same amount of copper—chooses such substrates with selectivities  $[\text{azide}(0)\text{alkyne}(-)]/[\text{azide}(0)\text{alkyne}(+)] = 35$  and  $[\text{alkyne}(0)\text{azide}(-)]/[\text{alkyne}(0)\text{azide}(+)] = 110$ . Error bars are standard deviations from three independent experiments (whose individual outcomes are quantified by gray markers in the histograms).

repulsions are as high as  $\sim 5$  kT per thiol such that formation of pure TMA patches (and, consequently, of pure Bipy patches over remaining areas) would cost several hundred kT's per nanoparticle. Fifth, the particles were stable to ca. 80 °C – at this temperature, some gradual coalescence/ripening of the NPs was observed though their zeta potentials as well as compositions of ligands shells determined by ICP-AES

remained similar to the initial particles (see SI, Section S8). Sixth, after completion of a catalysis run, the NPs could be reused for another round with similar results (see Figure S34).

Turning to the actual click reactions, we first tested whether the NPs can selectively catalyze click reactions depending on substrate charge (Figure 2a). For these comparisons, we chose pairs of alkynes/azides (Figure 2b) in which one was neutral, “0”, and one charged “+” or “−”; in this way, the electrostatic interactions were strictly between one of the substrates and the NP, and not between the substrates (still, for completeness, data for “++”, “− −”, “+−” and “−+” combinations are included in Figure S40). All reactions were monitored up to 24 h at r.t. Analyses of the reaction mixtures by  $^1\text{H}$  NMR summarized by the orange bars in Figure 2c and also kinetic plots in Figure 2d evidence that the conversions are high as long as one of the substrates bears negative charge (conversion  $98.8 \pm 0.52\%$  for “0−” and  $88.3 \pm 2.78\%$  for “−0”). In sharp contrast, when the azide or the alkyne are positively charged (“0+” and “+0”), the conversion drops to ca. 10%. This result echoes previous studies by us<sup>54</sup> and others<sup>55</sup> on the ability of TMA nanoparticles to admit negatively charged nitrophenol substrates—in those studies, however, nitrophenol was reduced at AuNP surfaces to a neutral aniline whereas, in our current system, charge is still present on the click reaction's products. The fact that conversions for “0−” and “−0” pairs are so high evidence not only that the positively charged NP attracts negatively charged substrates but also that negatively charged substrates and/or reaction products are not stuck in the TMA monolayer and are not “poisoning” the NP catalyst. Importantly, control experiments using equal amounts of copper free in water solution (as 0.46 mM  $\text{CuSO}_4/\text{NaAs}$ , where As = ascorbate) rather than on NPs demonstrate no similar selectivity. For the  $\text{CuSO}_4/\text{NaAs}$  system, all conversions are above 80% and as high as 97.4% for “−0” (green bars in Figure 2c and green curves in Figure 2d).

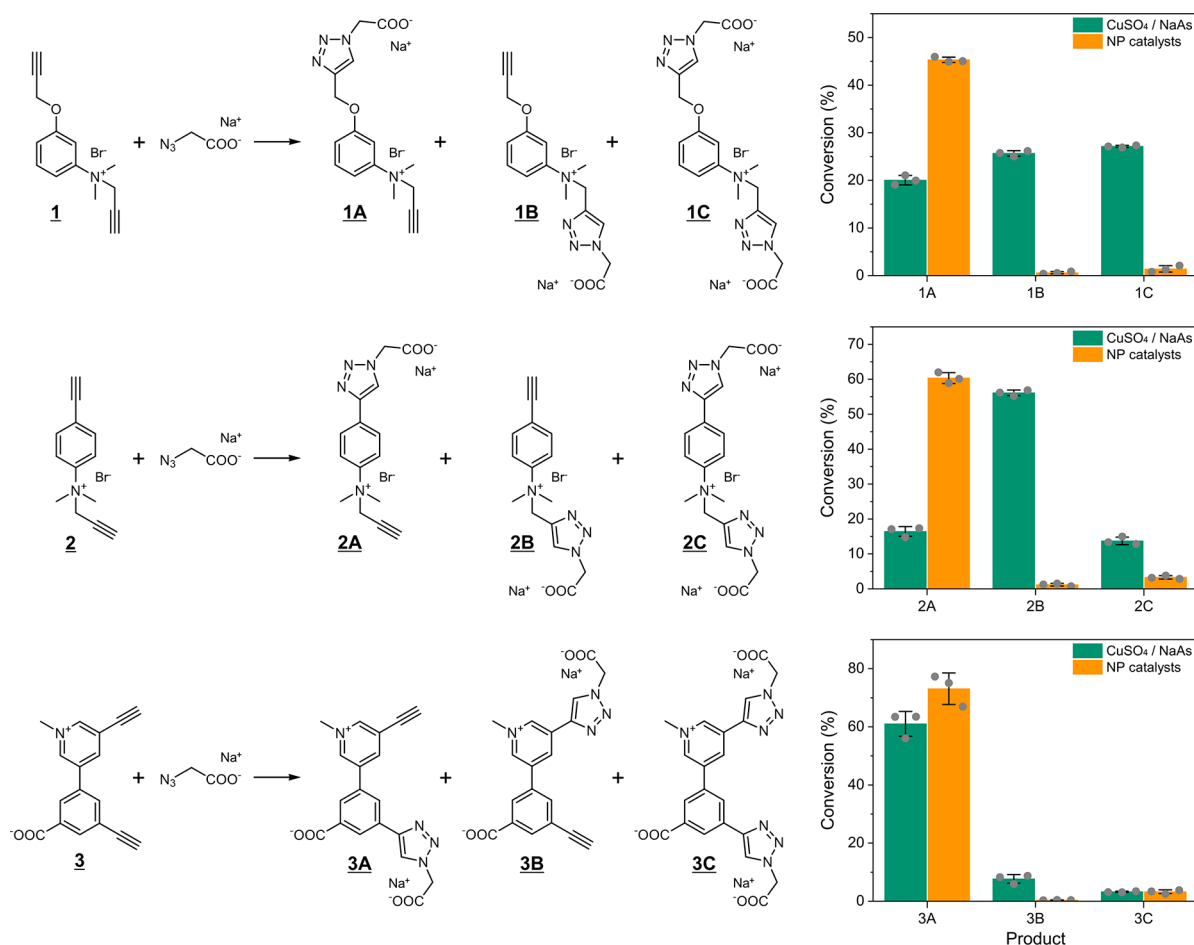


**Figure 4.** Site-selective, on-nanoparticle catalysis. (a) Substrates **1–3** and their possible products (singly reacted, A and B, and doubly reacted, C). Histograms quantify the distributions of these products at 24 h for CuSO<sub>4</sub>/NaAs catalysts (green bars) and for the NP-based catalysts (orange bars; same Cu concentration as for CuSO<sub>4</sub>/NaAs). NP-based catalysts exhibit strong preference for products A (cf. Figure 1c). Gray markers = results of individual experiments; error bars = standard deviations.

To further explore the selectivity of our NP catalysts, we performed a series of experiments analogous to enzymatic competitive-binding assays. In one example, we used a mixture of approximately equal amounts of a neutral azide(0), a negatively charged alkyne(−), and a positively charged alkyne(+) (entry 1 in Figure 3) and analyzed the reaction products obtained in the presence of either CuSO<sub>4</sub>/NaAs or our NP catalysts (both at 24 h and 80 °C to maximize conversions). In the first case, CuSO<sub>4</sub>/NaAs catalyzed indiscriminately both of the possible reactions, and the conversions for cycloadducts formed from azide(0)/alkyne(−) and azide(0)/alkyne(+) were similar (respectively, 46.9% and 51.7%). However, when Cu(I)-loaded AuNPs were used, the azide(0)/alkyne(−) product was formed in ca. 35-fold excess over the azide(0)/alkyne(+) one (93.1% yield vs 2.6%). Analogous results were observed when azide(−) and azide(+) competed for reaction with a neutral alkyne(0) (entry 2 in Figure 3) – for CuSO<sub>4</sub>/NaAs, there was only a slight preference for the azide(−)/alkyne(0) outcome but for NP catalysts, this preference was much more pronounced (110-fold; 95.5% vs 0.86%).

Arguably, the most important results are for the situation when the same substrate has two potentially reactive groups but one of them is closer to the charge-bearing group—we expected that in this situation, the electrostatic interaction

between the incoming substrate and gating/TMA charged groups could preorient the substrate such that the reactive group more distant from the charge center would enter the monolayer first and undergo the click reaction preferentially (see Figure 1c). To test this hypothesis, we synthesized substrates marked **1** through **3** bearing two terminal alkynes (Figure 4; for synthetic details, see SI, Section S5). For each of these substrates, reaction with an azide could lead to three possible products – “A” singly reacted at an alkyne further from the positively charged center, “B” singly reacted at an alkyne closer to the positively charged center, and “C” doubly reacted at both alkynes. As before, comparisons were made between CuSO<sub>4</sub>/NaAs catalysis (green bars) and on-nanoparticle catalysis (orange bars) at 24 h (for details, see SI, Section S6). As seen, for **1** through **3**, the use of NPs always increased the yield of product A and suppressed formation of B and C – this effect was observed irrespective of the native reactivity in the CuSO<sub>4</sub>/NaAs system (approximately equal distribution of products for **1**, favoring formation of B for **2**, or favoring formation of A for **3**).

The site-selectivities of the “gated” NPs for A, defined as a ratio of singly reacted products,  $S_{AB}^{NP} = [A]/[B]$ , are 74.8 for **1**, 51.3 for **2**, and 179.7 for **3**. This measure, however, neglects the doubly reacted product formed through A and B intermediates. Accordingly, using solutions to kinetic equations

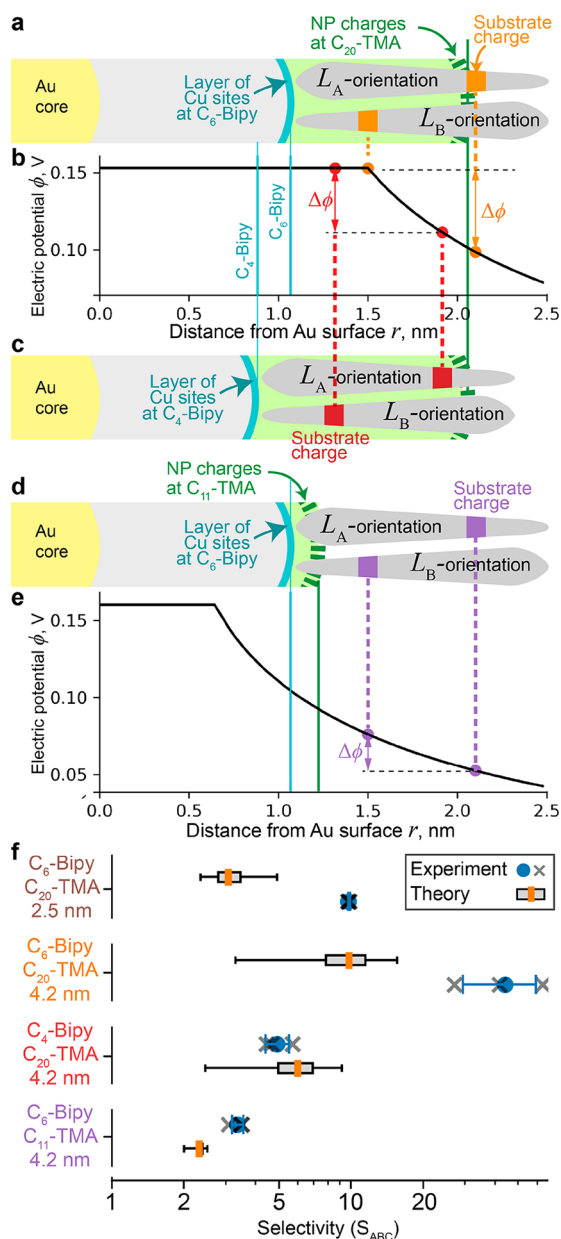


**Figure 5.** Theoretical model. (a, c, d) Charged nanoparticle with catalytic ligands (sky-blue) on its surface can be approached by a substrate molecule (gray pins) oriented in two different ways,  $L_A$  or  $L_B$ . (b, e) Black curves trace potentials due to longer ( $C_{20}$ ) or shorter ( $C_{11}$ ) gating TMA ligands (dark green). MD calculations (Figure S107) indicate that the effective radius at which the potential becomes approximately constant is shorter by ca. 0.6 nm than the average radius at which TMA's quaternary nitrogen groups reside. This correction is incorporated into the PB model. Colored points on the potential curves correspond to the potentials experienced by the incoming ligands reaching the Bipy centers in two possible orientations. Bipy centers are attached to NPs via (a, d) longer,  $C_6$  alkane, chains or (c) shorter,  $C_4$ , chains.  $\Delta$ 's are potential differences between  $L_A$  and  $L_B$ . (f) Comparison of theoretical and experimental selectivities,  $S_{ABC}$  for substrate **1** and various nanoparticles (indicated are lengths of Bipy and TMA ligands, as well as NP core size). Black crosses are data from individual experiments, blue dots are mean values, and blue error bars are standard deviations. Boxplots are theoretical predictions computed based on the real experimental distributions of NP sizes (see the SI, Section S10 for details). Boxplot elements are median (orange line), 25%, and 75% quartiles (box edges), maximum and minimum values (whiskers).

describing the kinetic system detailed in the SI Section S10, selectivity can be more accurately defined as  $S_{ABC} = \ln(1 + C)/[B] / \ln(1 + [C]/[A])$ , which reduces to  $[A]/[B]$  for small  $[C]$ . For NP catalysts,  $S_{ABC}^{NP}$  values are 44.2 for **1**, 26.3 for **2**, and 51 for **3**. Yet another way of expressing these selectivities is relative to the “native,”  $CuSO_4/NaAs$  values,  $S_{AB}^{rel} = S_{AB}^{AB}/S_{AB}^{Cu}$  and  $S_{ABC}^{rel} = S_{ABC}^{NP}/S_{ABC}^{Cu}$  such as to quantify the degree to which the NPs alone affect preferential product formation. These values are  $S_{AB}^{rel} = 95.8$  and  $S_{ABC}^{rel} = 52.3$  for **1**,  $S_{AB}^{rel} = 175.3$  and  $S_{ABC}^{rel} = 73.1$  for **2**, and  $S_{AB}^{rel} = 22.4$  and  $S_{ABC}^{rel} = 7.4$  for **3**.

While we do not attempt here to justify the native product distributions in the  $CuSO_4/NaAs$  system (as they may reflect a variety of factors, including details of coordination of the substrate to the catalytic center), a simple theoretical model can rationalize how the NPs impart the observed site-preference. In this model, we consider a reaction  $L + M \rightarrow Z$ , in which a charged dialkyne  $L$  can have two orientations with respect to the charged, catalytic surface of the nanoparticle (in Figure 5a,c,d denoted  $L_A$  and  $L_B$ , respectively;  $M$  stands for the azide). Depending on the orientation of  $L$ , two reaction “pathways” with pseudo-first-order reaction rates  $k_A[L_A]$  and  $k_B[L_B]$ , and two distinct, singly reacted products are then possible,  $L_A + M \rightarrow Z_A$  and  $L_B + M \rightarrow Z_B$  (these products can further react into disubstituted product C). Given certain probabilities  $P(L_A) = [L_A]/[L]$  and  $P(L_B) = [L_B]/[L]$  of molecule  $L$  to be oriented in two different ways near the catalytic surface of the nanoparticle, it can be shown (SI, Section S10) that reactions forming  $Z_A$  and  $Z_B$  are pseudo-first-order in  $[L]$  with rate constants  $\tilde{k}_A$  and  $\tilde{k}_B$  whose ratio is  $\tilde{k}_A/\tilde{k}_B = k_A P(L_A)/(k_B P(L_B)) = W \cdot P(L_A)/P(L_B)$ , where  $W = k_A/k_B$  is the “native” kinetic asymmetry between two reaction pathways. Making a reasonable assumption that these orientations in solution are thermally equilibrated, we can use Boltzmann distribution to obtain  $\tilde{k}_A/\tilde{k}_B = W \exp(-q(\phi(r_A) - \phi(r_B))/kT)$ , in which the difference in the energies of  $L_A$  and  $L_B$  is due to the electric potential  $\phi(r)$  of the charged nanoparticle and  $r = r_A$  in orientation  $L_A$ , or  $r = r_B$  in orientation  $L_B$ . The electric potential field  $\phi(r)$  is calculated by numerically solving full nonlinear Poisson–Boltzmann (PB) equation for our nanoparticles, whereas the values of  $r_A$  and  $r_B$  are estimated from Molecular Dynamics simulations (see SI, Sections S10.2 and S10.3). In relation to experiments,  $\tilde{k}_A/\tilde{k}_B$  is equal to experimental selectivity  $S_{ABC}$ , and approaches simple product ratio  $S_{AB} = [Z_A]/[Z_B]$  when disubstituted product is neglected. Despite the relative simplicity of this model, it accurately predicts the differences in kinetic rates in noncompetitive reactions from Figure 2d (see SI, Section S10.2) as well as the trends in selectivities  $S_{ABC}$  observed for particles harboring different ligands and/or having different core sizes (Figures 5f, 6a–c).

Specifically, an important parameter controlling selectivity is ligand length. Figure 6a summarizes experiments in which the lengths of the alkane chains were varied ( $C_4$  and  $C_6$  for Bipy and  $C_{11}$  and  $C_{20}$  for TMA thiols). As seen, the  $C_6$ –Bipy/ $C_{20}$ –TMA combination is more selective than either  $C_4$ –Bipy/ $C_{20}$ –TMA (larger length difference) or  $C_6$ –Bipy/ $C_{11}$ –TMA (smaller length difference). This result means that selectivity is not simply a function of the distance from the Bipy units to the TMA gating groups. On the other hand, the results are well explained by our electrostatic model. Specifically and with reference to Figure 5, Gauss' law necessitates that electric potential inside a charged spherical shell is uniform in the PB model (flat segments of black curves in Figure 5b,e). In order

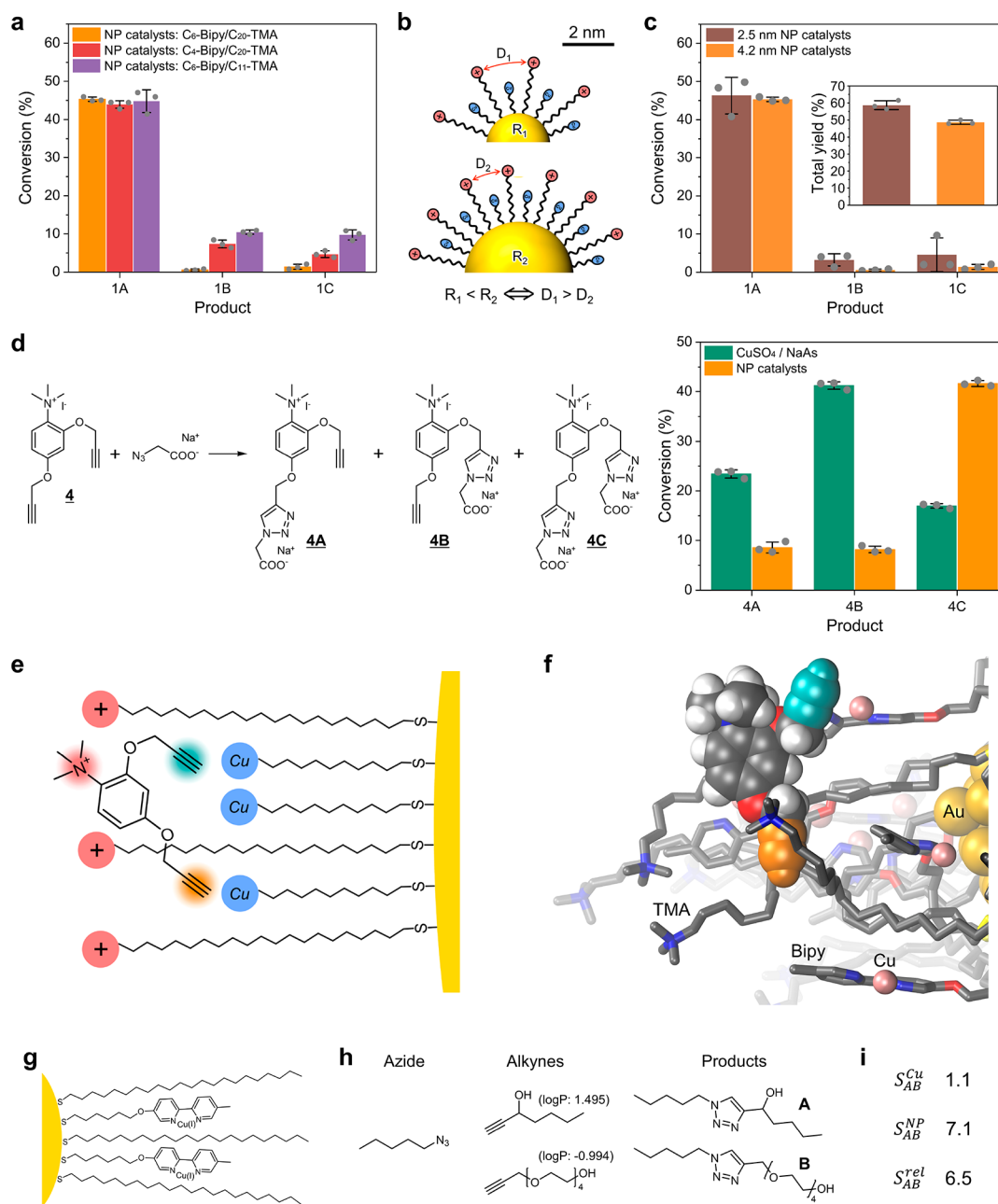


**Figure 6.** Different effects influencing gating and selectivity. (a) Experimentally measured conversions, into two singly reacted and one doubly reacted products, for the on-particle click reactions between a positively charged dialkyne **1** and a negatively charged azide (same as in Figure 4, 6.9 and 2.3 mM, respectively). The particles all have 4.2 nm Au cores but differ in the lengths of the Bipy and/or TMA ligands, as indicated in the legend. Reactions were performed at 80 °C and conversions were measured at 24 h. (b) Scheme illustrating that the distance between the gating, charged TMA groups decreases when the size of the nanoparticle increases. (c) Same reaction as in (a) but for nanoparticles differing in the size of Au cores. The concentrations of nanoparticles (10 μM for 2.5 nm NPs, 3.55 μM for 4.2 nm NPs) were such that the concentration of Bipy-Cu(I) catalytic units was approximately the same in both cases (0.46 mM). (d) Singly and doubly reacted products from dialkyne substrate **4**. The distributions of these products at 24 h (80 °C) are quantified in the rightmost column for CuSO<sub>4</sub>/NaAs catalysts (green bars) and for the NP-based catalysts (orange bars). In panels b, c, and d, error bars are standard deviations from three independent experiments (whose individual outcomes are quantified by gray markers in the histograms). (e) Scheme of pincer-like arrangement of **4** into the monolayer of NP catalysts. (f) Corresponding snapshot from MD simulation. (g) A proof-of-the-principle example of hydrophobic/hydrophilic gating by *n*-alkane, C<sub>22</sub> ligands surrounding the catalytic centers on the particle. (h) Among the reaction substrates, the two alkynes were chosen such that they (1) were both soluble in CHCl<sub>3</sub> yet (2) differed in the phobicity of their *n*-alkane vs tetra(ethylene glycol) “tails”. These substrates competed for the reaction with the azide partner shown. The two possible products that can form are, correspondingly, labeled as A and B. (i) In the CuSO<sub>4</sub>/NaAs system, there is no selectivity, and A and B form in roughly equal proportions. In contrast, with Cu-Bipy/NP catalysts, the alkyne with *n*-alkane tail enters the hydrophobic monolayer preferentially and gives product A in 7-fold excess. For all synthetic details, see the SI, Section S11.

to reach the Cu atom of C<sub>4</sub>-Bipy (Figure 5c), the dialkyne must approach the Au core closer than in the case of C<sub>6</sub>-Bipy (Figure 5a); this corresponds to a horizontal shift between red

and orange pairs of points in Figure 5b on a shared potential curve (defined by TMA ligand length and NP size). As a consequence, the charged group of dialkyne in orientation L<sub>A</sub>

(left red point in Figure 5b) must enter the region of constant potential in order to react, and therefore, the potential difference  $\Delta\phi$  between  $L_A$  and  $L_B$  is reduced relative to the  $C_6$ -Bipy case. Because selectivity depends exponentially on  $\Delta\phi$ , it follows the same trend (Figure 5f). Along similar lines, for a constant alkane chain length ( $C_6$ ) of Bipy ligand, a change from  $C_{20}$ -TMA to a shorter  $C_{11}$ -TMA shifts the potential curve toward the Au core (Figure 5a,b vs d,e). The dialkyne substrate can now reach the Cu site at  $C_6$ -Bipy while being largely outside the layer of  $C_{11}$ -TMA quaternary nitrogens (green in Figure 5d,e) where the potential is less steep. Thus,  $\Delta\phi$  is reduced (Figure 5e, purple points) relative to the  $C_6$ -Bipy/ $C_{20}$ -TMA case and selectivity drops accordingly (Figure 5f, bottom).

The effect of NP size also merits an additional comment. On one hand, when the NPs become larger and their curvature decreases, the thiol monolayers fan out less and form a more tightly packed monolayer in which the access to the catalytic centers is sterically restricted (Figure 6b), possibly compromising the total yield. Indeed, as seen in Figure 6c, the total yield for 4.2 nm NPs is  $\sim 10\%$  lower than for 2.5 nm NPs (in these two cases, the NP concentrations were adjusted such that the concentration of Bipy-Cu(I) was constant, 0.46 mM and 20% of substrates' concentration). On the other hand, NP's surface electric potential  $\phi(r)$  increases with particle size, in turn increasing the magnitude of the electric potential energy difference ( $\phi(r_A) - \phi(r_B)$ ) between the two orientations of a substrate and therefore improving the selectivity by  $\sim \exp(-q(\phi(r_A) - \phi(r_B))/kT)$ ; this effect is, indeed, seen in the distribution of products shown in Figure 6c.

Finally, we would like to emphasize that despite the apparent simplicity of the NPs we used, the dynamics of the monolayer/catalytic center/substrate system can be nuanced. In particular, the selectivities observed for some substrates cannot be predicted "by inspection" and, instead, careful modeling is needed to understand the experimental outcomes, in some sense strengthening the analogy to enzymes, for which understanding substrate binding and reactivity also benefits from simulations. As a case in point, we synthesized the substrate marked **4** in Figure 6d; in this molecule, the charged group is only slightly closer to one of the two alkynes. Although we expected that this smaller difference might result in decreased selectivity between **4A** and **4B**, we were surprised to find that the main effect was a dramatically increased formation of the disubstituted product **4C** (in a  $\sim 5:2$  ratio with respect to the sum of singly reacted products; see orange bars in Figure 6d). This effect is clearly due to the NP since, in the  $CuSO_4/NaAs$  system, singly reacted products **4A** and **4B** are dominant. Also, in the NP system, the 5:2 product ratio is established already within  $\sim 1$  h, suggesting that reactions on both alkynes happen in rapid succession. These results can be rationalized by MD simulations illustrated in Figure 6e,f (and detailed in the SI, Section S10.3), namely, the substrate orients such that the charged  $NMe_3^+$  group on the phenyl ring is pointing away from the NP whereas the two alkynes arrange in a pincer-like fashion such that they can both enter the on-particle monolayer and react on the catalytic sites within it.

## CONCLUSIONS

In summary, ligands self-assembling on the surface of nanoparticles can create "active sites" controlling access to catalytic units and preorganizing the incoming substrates for selective reactions at only some of otherwise similar-reactivity

sites. We see this approach as a form of "enhancing" known catalysts to endow them with new selectivity modalities—in addition to the electrostatic gating described here, we envision, for instance, that hydrophilic/hydrophobic gating ligands could differentiate substrate sites based on the polarity of nearby groups (see proof-of-the concept experiments in Figure 6g–i), while chiral ligands could control access of select enantiomers. An unexplored but promising aspect of this work would be to also harness the properties of the NP core, e.g., to retrieve from reaction mixture catalysts tethered onto magnetic particles or to couple Ir or Ru-based photoredox catalysts to the plasmonic response of AuNPs.

## ASSOCIATED CONTENT

### Supporting Information

The Supporting Information is available free of charge at <https://pubs.acs.org/doi/10.1021/jacs.0c09408>.

Synthetic and experimental details and NMR data, computational details, and simulation results (PDF)

## AUTHOR INFORMATION

### Corresponding Author

Bartosz A. Grzybowski — Center for Soft and Living Matter, Institute for Basic Science (IBS), Ulsan, Republic of Korea; Department of Chemistry, Ulsan National Institute of Science and Technology (UNIST), Ulsan, Republic of Korea; Institute of Organic Chemistry, Polish Academy of Sciences, Warsaw, Poland; [orcid.org/0000-0001-6613-4261](https://orcid.org/0000-0001-6613-4261); Email: [nanogrzybowski@gmail.com](mailto:nanogrzybowski@gmail.com)

### Authors

Minju Kim — Center for Soft and Living Matter, Institute for Basic Science (IBS), Ulsan, Republic of Korea; Department of Chemistry, Ulsan National Institute of Science and Technology (UNIST), Ulsan, Republic of Korea  
Miroslaw Dygas — Center for Soft and Living Matter, Institute for Basic Science (IBS), Ulsan, Republic of Korea; Institute of Organic Chemistry, Polish Academy of Sciences, Warsaw, Poland  
Yaroslav I. Sobolev — Center for Soft and Living Matter, Institute for Basic Science (IBS), Ulsan, Republic of Korea  
Wiktor Beker — Institute of Organic Chemistry, Polish Academy of Sciences, Warsaw, Poland  
Qiang Zhuang — Center for Soft and Living Matter, Institute for Basic Science (IBS), Ulsan, Republic of Korea; School of Chemistry and Chemical Engineering, Northwestern Polytechnical University, Xi'an, China  
Tomasz Klucznik — Institute of Organic Chemistry, Polish Academy of Sciences, Warsaw, Poland  
Guillermo Ahumada — Center for Soft and Living Matter, Institute for Basic Science (IBS), Ulsan, Republic of Korea; [orcid.org/0000-0002-1507-0816](https://orcid.org/0000-0002-1507-0816)  
Juan Carlos Ahumada — Center for Soft and Living Matter, Institute for Basic Science (IBS), Ulsan, Republic of Korea

Complete contact information is available at: <https://pubs.acs.org/doi/10.1021/jacs.0c09408>

### Author Contributions

M.K. designed and performed most experiments and analyzed the data. M.D., G.A., and J.C.A. synthesized ligand molecules for nanoparticles. Y.S. developed theoretical models and conducted data analysis. W.B. performed molecular dynamics

(MD) simulation and related analysis. Q.Z. optimized nanoparticle functionalization and performed some experiments. M.K., M.D., Q.Z., T.K., G.A., and J.C.A. synthesized substrates used for catalysis. G.A. and J.C.A. performed experiments on hydrophobic gating. B.A.G. conceived and supervised the research. B.A.G. wrote the manuscript with help from other authors, mostly M.K., Y.S., and W.B. All authors discussed the results and corrected the manuscript.

## Notes

The authors declare no competing financial interest.

## ACKNOWLEDGMENTS

This work was supported by the Institute for Basic Science, Republic of Korea (IBS-R020-D1) and by the National Science Center, Poland (Grant Maestro, No. 2018/30/A/ST5/00529).

## REFERENCES

- (1) Berg, J. M.; Tymoczko, J. L.; Stryer, L. *Biochemistry*, 6th ed.; W. H. Freeman and Company: New York, 2006.
- (2) Davis, H. J.; Phipps, R. J. Harnessing non-Covalent Interactions to Exert Control over Regioselectivity and Site-Selectivity in Catalytic Reactions. *Chem. Sci.* **2017**, *8*, 864–877.
- (3) Meeuwissen, J.; Reek, J. H. H. Supramolecular Catalysis beyond Enzyme Mimics. *Nat. Chem.* **2010**, *2*, 615–621.
- (4) Margelefsky, E. L.; Zeidan, R. K.; Davis, M. E. Heterogeneous Catalyst Design by Multiple Functional Group Positioning in Organic-Inorganic Materials: On the Route to Analogs of Multifunctional Enzymes. In *Model Systems in Catalysis: Single Crystals to Supported Enzyme Mimics*; Springer: New York, 2010; pp 495–516.
- (5) Jones, C. W.; Tsuji, K.; Davis, M. E. Organic-Functionalized Molecular Sieves as Shape-Selective Catalysts. *Nature* **1998**, *393*, 52–54.
- (6) Nishioka, Y.; Yamaguchi, T.; Yoshizawa, M.; Fujita, M. Unusual [2 + 4] and [2 + 2] Cycloadditions of Arenes in the Confined Cavity of Self-Assembled Cages. *J. Am. Chem. Soc.* **2007**, *129*, 7000–7001.
- (7) Bhawe, Y.; Moliner-Marín, M.; Lunn, J. D.; Liu, Y.; Malek, A.; Davis, M. Effect of Cage Size on the Selective Conversion of Methanol to Light Olefins. *ACS Catal.* **2012**, *2*, 2490–2495.
- (8) Murase, T.; Horiuchi, S.; Fujita, M. Naphthalene Diels-Alder in a Self-Assembled Molecular Flask. *J. Am. Chem. Soc.* **2010**, *132*, 2866–2867.
- (9) Mock, W. L.; Irra, T. A.; Wepsiec, J. P.; Manimaran, T. L. Cycloaddition Induced by Cucurbituril. A Case of Pauling Principle Catalysis. *J. Org. Chem.* **1983**, *48*, 3619–3620.
- (10) Jon, S. Y.; Ko, Y. H.; Park, S. H.; Kim, H. J.; Kim, K. A Facile, Stereoselective [2 + 2] Photoreaction Mediated by Cucurbit[8]uril. *Chem. Commun.* **2001**, *19*, 1938–1939.
- (11) Chen, J.; Rebek, J. Selectivity in an Encapsulated Cycloaddition Reaction. *Org. Lett.* **2002**, *4*, 327–329.
- (12) Kang, J. M.; Santamaria, J.; Hilmersson, G.; Rebek, J. Self-Assembled Molecular Capsule Catalyzes a Diels-Alder Reaction. *J. Am. Chem. Soc.* **1998**, *120*, 7389–7390.
- (13) Kuil, M.; Soltner, T.; van Leeuwen, P.; Reek, J. N. H. High-Precision Catalysts: Regioselective Hydroformylation of Internal Alkenes by Encapsulated Rhodium Complexes. *J. Am. Chem. Soc.* **2006**, *128*, 11344–11345.
- (14) Merlau, M. L.; del Pilar Mejía, M.; Nguyen, S. T.; Hupp, J. T. Artificial Enzymes Formed Through Directed Assembly of Molecular Square Encapsulated Epoxidation Catalysts. *Angew. Chem., Int. Ed.* **2001**, *40*, 4239–4242.
- (15) Slagt, V. F.; Roder, M.; Kamer, P. C. J.; van Leeuwen, P.; Reek, J. N. H. Supraphos: A Supramolecular Strategy to Prepare Bidentate Ligands. *J. Am. Chem. Soc.* **2004**, *126*, 4056–4057.
- (16) Dydio, P.; Dzik, W. I.; Lutz, M.; de Bruin, B.; Reek, J. N. H. Remote Supramolecular Control of Catalyst Selectivity in the Hydroformylation of Alkenes. *Angew. Chem., Int. Ed.* **2011**, *50*, 396–400.
- (17) Leung, D. H.; Bergman, R. G.; Raymond, K. N. Highly Selective Supramolecular Catalyzed Allylic Alcohol Isomerization. *J. Am. Chem. Soc.* **2007**, *129*, 2746–2747.
- (18) Yoshizawa, M.; Tamura, M.; Fujita, M. Diels-Alder in Aqueous Molecular Hosts: Unusual Regioselectivity and Efficient Catalysis. *Science* **2006**, *312*, 251–254.
- (19) Pluth, M. D.; Bergman, R. G.; Raymond, K. N. Acid Catalysis in Basic Solution: A Supramolecular Host Promotes Orthoformate Hydrolysis. *Science* **2007**, *316*, 85–88.
- (20) Davis, M. E. New Vistas in Zeolite and Molecular Sieve Catalysis. *Acc. Chem. Res.* **1993**, *26*, 111–115.
- (21) Wight, A. P.; Davis, M. E. Design and Preparation of Organic-Inorganic Hybrid Catalysts. *Chem. Rev.* **2002**, *102*, 3589–3614.
- (22) Margelefsky, E. L.; Zeidan, R. K.; Davis, M. E. Cooperative Catalysis by Silica-Supported Organic Functional Groups. *Chem. Soc. Rev.* **2008**, *37*, 1118–1126.
- (23) Tsuji, K.; Jones, C. W.; Davis, M. E. Organic-Functionalized Molecular Sieves (OFMSs): I. Synthesis and Characterization of OFMSs with Polar Functional Groups. *Microporous Mesoporous Mater.* **1999**, *29*, 339–349.
- (24) Jones, C. W.; Tsuji, K.; Davis, M. E. Organic-Functionalized Molecular Sieves (OFMSs): II. Synthesis, Characterization and the Transformation of OFMSs Containing Non-Polar Functional Groups into Solid Acids. *Microporous Mesoporous Mater.* **1999**, *33*, 223–240.
- (25) Jones, C. W.; Hwang, S.-J.; Okubo, T.; Davis, M. E. Synthesis of Hydrophobic Molecular Sieves by Hydrothermal Treatment with Acetic Acid. *Chem. Mater.* **2001**, *13*, 1041–1050.
- (26) Breslow, R.; Zhang, X.; Huang, Y. Selective Catalytic Hydroxylation of a Steroid by an Artificial Cytochrome P-450 Enzyme. *J. Am. Chem. Soc.* **1997**, *119*, 4535–4536.
- (27) Yang, J.; Breslow, R. Selective Hydroxylation of a Steroid at C-9 by an Artificial Cytochrome P-450. *Angew. Chem., Int. Ed.* **2000**, *39*, 2692–2694.
- (28) Fang, Z.; Breslow, R. Metal Coordination-Directed Hydroxylation of Steroids with a Novel Artificial P-450 Catalyst. *Org. Lett.* **2006**, *8*, 251–254.
- (29) Dydio, P.; Ploeger, M.; Reek, J. N. H. Selective isomerization-hydroformylation sequence: A Strategy to Valuable  $\alpha$ -Methyl-Branched Aldehydes from Terminal Olefins. *ACS Catal.* **2013**, *3*, 2939–2942.
- (30) Dydio, P.; Reek, J. N. H. Supramolecular control of selectivity in hydroformylation of vinyl arenes: Easy Access to Valuable  $\beta$ -aldehyde Intermediates. *Angew. Chem., Int. Ed.* **2013**, *52*, 3878–3882.
- (31) Dydio, P.; Reek, J. N. H. Supramolecular Control of Selectivity in Transition-Metal Catalysis through Substrate Preorganization. *Chem. Sci.* **2014**, *5*, 2135–2145.
- (32) Qing, Y.; Tamagaki-Asahina, H.; Ionescu, S. A.; Liu, M. D.; Bayley, H. Catalytic Site-Selective Substrate Processing within a Tubular Nanoreactor. *Nat. Nanotechnol.* **2019**, *14*, 1135–1142.
- (33) Wu, J.; Wang, X.; Wang, Q.; Lou, Z.; Li, S.; Zhu, Y.; Qin, L.; Wei, H. Nanomaterials with Enzyme-Like Characteristics (nanozymes): Next-Generation Artificial Enzymes (II). *Chem. Soc. Rev.* **2019**, *48*, 1004–1076.
- (34) Liang, M.; Yan, X. Nanozymes: From New Concepts, Mechanisms, and Standards to Applications. *Acc. Chem. Res.* **2019**, *52*, 2190–2200.
- (35) Wang, H.; Wan, K.; Shi, X. Recent Advances in Nanozyme Research. *Adv. Mater.* **2019**, *31*, 1805368.
- (36) Zhang, Z. J.; Zhang, X. H.; Liu, B. W.; Liu, J. W. Molecular Imprinting on Inorganic Nanozymes for Hundred-Fold Enzyme Specificity. *J. Am. Chem. Soc.* **2017**, *139*, 5412–5419.
- (37) Phan, N. T. S.; Van Der Sluys, M.; Jones, C. W. On the Nature of the Active Species in Palladium Catalyzed Mizoroki-Heck and Suzuki-Miyaura Couplings - Homogeneous or Heterogeneous Catalysis, A Critical Review. *Adv. Synth. Catal.* **2006**, *348*, 609–679.
- (38) Fillon, Y.; Verma, A.; Ghosh, P.; Ermenwein, D.; Rotello, V. M.; Chmielewski, J. Peptide Ligation Catalyzed by Functionalized Gold Nanoparticles. *J. Am. Chem. Soc.* **2007**, *129*, 6676–6677.

(39) Zaramella, D.; Scrimin, P.; Prins, L. J. Self-Assembly of a Catalytic Multivalent Peptide-Nanoparticle Complex. *J. Am. Chem. Soc.* **2012**, *134*, 8396–8399.

(40) Jin, L.; Liu, B.; Duay, S. S.; He, J. Engineering Surface Ligands of Noble Metal Nanocatalysts in Tuning the Product Selectivity. *Catalysts* **2017**, *7*, 44.

(41) Tonga, G. Y.; Jeong, Y.; Duncan, B.; Mizuhara, T.; Mout, R.; Das, R.; Kim, S. T.; Yeh, Y.-C.; Yan, B.; Hou, S.; Rotello, V. M. Supramolecular Regulation of Bioorthogonal Catalysis in Cells using Nanoparticle-Embedded Transition Metal Catalysts. *Nat. Chem.* **2015**, *7*, 597–603.

(42) Neri, S.; Garcia Martin, S.; Pezzato, C.; Prins, L. J. Photoswitchable Catalysis by a Nanozyme Mediated by a Light-Sensitive Cofactor. *J. Am. Chem. Soc.* **2017**, *139*, 1794–1797.

(43) Prins, L. J. Emergence of Complex Chemistry on an Organic Monolayer. *Acc. Chem. Res.* **2015**, *48*, 1920–1928.

(44) Love, J. C.; Estroff, L. A.; Kriebel, J. K.; Nuzzo, R. G.; Whitesides, G. M. Self-Assembled Monolayers of Thiolates on Metals as a Form of Nanotechnology. *Chem. Rev.* **2005**, *105*, 1103–1169.

(45) Yan, Y.; Warren, S. C.; Fuller, P.; Grzybowski, B. A. Chemoelectronic Circuits Based on Metal Nanoparticles. *Nat. Nanotechnol.* **2016**, *11*, 603–608.

(46) Kolb, H. C.; Finn, M. G.; Sharpless, K. B. Click Chemistry: Diverse Chemical Function from a Few Good Reactions. *Angew. Chem., Int. Ed.* **2001**, *40*, 2004–2021.

(47) Lewis, W. G.; Magallon, F. G.; Fokin, V. V.; Finn, M. G. Discovery and Characterization of Catalysts for Azide-Alkyne Cycloaddition by Fluorescence Quenching. *J. Am. Chem. Soc.* **2004**, *126*, 9152–9153.

(48) Hein, J. E.; Fokin, V. V. Copper-Catalyzed Azide-Alkyne Cycloaddition (CuAAC) and Beyond: New Reactivity of Copper(I) Acetylides. *Chem. Soc. Rev.* **2010**, *39*, 1302–1315.

(49) Borukhov, I.; Andelman, D.; Orland, H. Steric Effects in Electrolytes: A Modified Poisson-Boltzmann Equation. *Phys. Rev. Lett.* **1997**, *79*, 435–438.

(50) Kilib, M. S.; Bazant, M. Z.; Ajdari, A. Steric Effects in the Dynamics of Electrolytes at Large Applied Voltages. I. Double-Layer Charging. *Phys. Rev. E* **2007**, *75*, 021502.

(51) Rodionov, V. O.; Presolski, S. I.; Diaz Diaz, D.; Fokin, V. V.; Finn, M. G. Ligand-Accelerated Cu-Catalyzed Azide-Alkyne Cycloaddition: A Mechanistic Report. *J. Am. Chem. Soc.* **2007**, *129*, 12705–12712.

(52) Ahlquist, M.; Fokin, V. V. Enhanced Reactivity of Dinuclear Copper(I) Acetylides in Dipolar Cycloadditions. *Organometallics* **2007**, *26*, 4389–4391.

(53) Straub, B. F.  $\mu$ -Acetylide and  $\mu$ -Alkenylidene Ligands in “click” Triazole Syntheses. *Chem. Commun.* **2007**, *37*, 3868–3870.

(54) Zhuang, Q.; Yang, Z.; Sobolev, Y. I.; Beker, W.; Kong, J.; Grzybowski, B. A. Control and Switching of Charge-Selective Catalysis on Nanoparticles by Counterions. *ACS Catal.* **2018**, *8*, 7469–7474.

(55) Roy, S.; Rao, A.; Devatha, G.; Pillai, P. P. Revealing the Role of Electrostatics in Gold-Nanoparticle-Catalyzed Reduction of Charged Substrates. *ACS Catal.* **2017**, *7*, 7141–7145.